JOURNAL OF GEOPHYSICAL RESEARCH, VOL. 111, E06005, doi:10.1029/2005JE002519, 2006

Volcanic deposits in shield fields and highland regions on Venus: Surface properties from radar polarimetry

Lynn M. Carter,[1] Donald B. Campbell,[2] and Bruce A. Campbell[1]

Received 28 June 2005; revised 1 March 2006; accepted 7 March 2006; published 10 June 2006.

[1] We compare Arecibo dual-polarization radar image data for Venus to Magellan images and emissivity data to investigate the physical properties of volcanic deposits. Radar waves can easily penetrate smooth mantling layers such as ash, aeolian and crater-derived deposits. If a circularly polarized radar wave refracts into a surface that is smooth at wavelength scales, the vertical component of the wave will be preferentially transmitted, resulting in a net linear-polarized echo component. Arecibo polarimetry data were used to create maps of the degree of linear polarization in the radar echo. We find that some volcanic fields in plains regions on Venus are associated with enhanced linear polarization. These fields sometimes have nearby windstreaks which suggest fine-grained surface material, and we infer that the radar wave is penetrating into mantling deposits that are a few centimeters to ~1 m thick. Enhanced linear polarization values are also correlated with specific lava flows. These lava flows have emissivity values of 0.80 to 0.84, similar to many other flows on Venus. The enhanced linear polarization may be produced by penetration of the radar wave into very smooth lava flows with internal air gaps. High-reflectivity, low-emissivity areas near the summits of Theia and Tepev Montes also have a linearly polarized echo component consistent with surface penetration by the radar wave. The cause of the high linear polarization in summit regions remains uncertain, but perhaps the radar wave is able to penetrate into high dielectric material in limited cases of very smooth surface texture.

Citation: Carter, L. M., D. B. Campbell, and B. A. Campbell (2006), Volcanic deposits in shield fields and highland regions on Venus: Surface properties from radar polarimetry, *J. Geophys. Res.*, *111*, E06005, doi:10.1029/2005JE002519.

1. Introduction

[2] Studies of the morphology and radar properties of volcanic deposits can aid in understanding their formation and post-emplacement evolution. On Venus, volcanoes range in size from large highland edifices, such as Theia Mons, to small shields and domes. Large volcanoes (>100 km in diameter) are surrounded by radial flows which can be several hundreds of kilometers in length [*Crumpler et al.*, 1997]. Volcanic fields containing tens to hundreds of shield volcanoes with diameters less than 20 km are often surrounded by radar bright and dark lava flows [*Addington*, 2001; *Crumpler et al.*, 1997].

[3] Previous analysis of lava flows on Venus has shown that most are fairly smooth. *Campbell and Campbell* [1992] compared Arecibo dual-circular polarization data, NASA/JPL AIRSAR data of terrestrial sites, and Magellan data to show that volcanic deposits in Western Eistla Region (Sif and Gula Mons) and Northern Sedna Planitia have roughness properties similar to those of smooth, pahoehoe-type lavas. Magellan emissivity values for lava flows vary considerably and have led to the discovery of flows with interesting radar properties. For example, radar dark flows extending north from the summit of Kali Mons have very high (~0.9) emissivities [*Campbell and Clark*, 2005], as do localized regions on the flanks of Tepev Mons [*Campbell and Rogers*, 1994] and Maat Mons [*Pettengill et al.*, 1992]. Summit regions typically have low emissivities thought to be caused by altitude-dependent deposition or formation of a high dielectric material [*Pettengill et al.*, 1992, 1996; *Schaefer and Fegley*, 2004].

[4] There are not many examples of possible pyroclastic deposits in Magellan data, but ash deposits have been proposed in a few areas. The low-emissivity area on Maat Mons is one potential area of low dielectric constant pyroclastics [*Campbell*, 1994]. Studies of Bell Regio suggest the presence of fine-grained material in a low dielectric constant triangular-shaped region on the flank of Tepev Mons, which may be crater ejecta or a pyroclastic deposit spread westward by wind [*Campbell and Rogers*, 1994]. The eastern caldera on Tepev Mons shows a shallow slope in backscattered radar power versus incidence angle at low incidence angles, implying a fine-grained covering such as

[1]Center for Earth and Planetary Studies, Smithsonian Institution, Washington, D. C., USA.
[2]Department of Astronomy, Cornell University, Ithaca, New York, USA.

0148-0227/06/2005JE002519$09.00

ash [*Campbell and Rogers*, 1994]. Shield volcanoes in a field at 22°N, 332°E have radar dark haloes ~10 km in diameter that have been interpreted as possible pyroclastic deposits [*Head et al.*, 1991; *Guest et al.*, 1992].

[5] The high pressures and temperatures on Venus will prevent the formation of pyroclastic deposits unless the magma contains large amounts of volatiles [*Fagents and Wilson*, 1995; *Head and Wilson*, 1986]. *Fagents and Wilson* [1995] model the eruption process on Venus and show that the higher atmospheric pressure and lower subsurface pressure gradients on Venus will inhibit exsolution of volatiles and prevent explosive eruptions. If pyroclastic activity does occur, the dense, hot atmosphere will stop the eruption cloud from rising to the heights typically achieved on Earth, and the resulting pyroclastic deposit will be less widely distributed, ~5 km in diameter for volatile contents similar to terrestrial volcanoes [*Fagents and Wilson*, 1995].

[6] Radar waves can penetrate smooth mantling layers such as ash and aeolian deposits. If a radar system can measure the echo power in two orthogonal polarizations, it is possible to measure an enhancement of the vertically (V) polarized radar echo in cases where the radar wave is refracted into the surface and reflects off subsurface rocks or an underlying surface layer. The Magellan spacecraft could only measure horizontally (H) polarized radiation with the exception of a few orbits where the spacecraft was rotated to measure V polarization. Therefore, for most areas, Magellan was not able to fully characterize the polarization state of the radar echoes.

[7] Ground-based radars are normally capable of measuring the echo power in two orthogonal polarizations. Analysis of linear polarization has been used to constrain models of the lunar surface and dielectric constant [*Hagfors and Evans*, 1968] and to study surface properties near lunar impact craters [*Campbell et al.*, 1992]. *Stacy* [1993] mapped the fraction of linear polarized echo power in lunar polar regions and maria, and modeled the data to estimate the relative amounts of scattering from the surface and subsurface. *Carter et al.* [2004] used Arecibo 12.6-cm-wavelength radar data to show that the terrain around many impact craters on Venus has an enhanced linear polarization signature indicative of subsurface scattering. The 12–16 km/pixel Arecibo polarimetry can be compared to Magellan altimetry, emissivity, and high-resolution (150 m) SAR image data. The high degree of linear polarization values are usually correlated with diffuse, radar bright areas in the Magellan imagery. The increase in backscatter cross section is likely due to subsurface scattering from buried rocks or from a rough, mantled substrate. In this paper we utilize the same Venus data set to investigate surface physical properties of volcanic fields, lava flows, and highland volcanoes.

2. Arecibo Dual-Polarization Radar Data

[8] The degree of linear polarization maps were created using the Arecibo Observatory 12.6-cm-wavelength radar. Data were taken during inferior conjunctions of Venus in 1999, 2001, and 2004. Details of the 1999 and 2001 observations and data processing are given by *Carter et al.* [2004], and all of the observations are summarized in Table 1. A brief summary of the data processing is given here. Note that although the subradar latitude varies north and south of the equator, the subradar longitudes for each conjunction are similar. We are therefore only able to map part of the Venus surface centered around ~335° longitude using Earth-based radar.

Table 1. Summary of Arecibo Venus Observations

	15–27 August 1999	27–30 March 2001	3–5 June 2004
Subradar point	8.8°N, 332°E	9.2°S, 338°E	1.5°S, 332°E
Radar time resolution	4.2 μs	8.0 μs	8.0 μs
Range resolution	0.63 km	1.2 km	1.2 km
Final (averaged) resolution	16 km	12 km	12 km

[9] For each transmit/receive cycle (lasting about 10 min), delay-Doppler images of both received circular polarizations were combined to create maps in each of the four Stokes polarization parameters. The Stokes parameters can be used to completely describe the polarization state of a wave [*Jackson*, 1999], and for circularly polarized waves they are given by

$$S = \begin{bmatrix} S_1 \\ S_2 \\ S_3 \\ S_4 \end{bmatrix} = \begin{bmatrix} \langle |E_L|^2 \rangle + \langle |E_R|^2 \rangle \\ 2Re\langle E_L E_R^* \rangle \\ 2Im\langle E_L E_R^* \rangle \\ \langle |E_L|^2 \rangle - \langle |E_R|^2 \rangle \end{bmatrix}, \quad (1)$$

where E_L and E_R are the electric fields for the left and right circular polarizations respectively. The first Stokes parameter (S_1) is a measure of the total average power of the echo. The second and third Stokes parameters (S_2 and S_3) measure the linearly polarized power in two directions rotated by 45°. The S_4 Stokes parameter gives the direction and magnitude of the circularly polarized power. Stokes parameter images from multiple (11–17) receive intervals were combined and spatially averaged to improve signal-to-noise.

[10] A circularly polarized wave can be thought of as a combination of two orthogonal linear vectors that are vertically (V) and horizontally (H) polarized. If this wave penetrates into the surface, the V component will be preferentially transmitted, and the polarization state will change from circular to elliptical. The elliptical wave can be thought of as a combination of circularly polarized echo power and a linearly polarized component that has a measurable magnitude and direction. The degree (or percent) of linear polarization in the received echo can be defined as

$$m_l = \frac{\sqrt{S_2^2 + S_3^2}}{S_1}. \quad (2)$$

[11] The long axis of the polarization ellipse indicates the direction of the linear polarization vector. The angle of this long axis, with respect to the H polarization, is given by

$$\chi = \frac{1}{2} \arctan\left(\frac{S_3}{S_2}\right). \quad (3)$$

For subsurface scattering, the direction of the linear polarization will be parallel to the plane of incidence and reflection. Linear polarization can also be created by double-bounce surface reflections [*Campbell et al.*, 1992; *Stacy*, 1993]; however, in this case the polarization angle will be oriented 90° to the plane of incidence. The measured χ values were calibrated in order to link the raw-data angles with plane-of-sky position angles that could be compared to what is expected from subsurface scattering. Appendix A describes this calibration and shows the results for the 2004 data set. The calibrated polarization angles from our data show that the linear polarization lies in the plane of incidence, as is expected from surface penetration.

[12] Northern and southern hemisphere Mercator-projection maps of S_1, m_l and χ were created for each of the three observing years. The data were spatially averaged to improve signal-to-noise such that the final resolutions are 16 km for the data taken in 1999, and 12 km for the data taken in 2001 and 2004. There are three main sources of error in the m_l values: cross coupling of the polarizations, statistical Rice noise related to squaring the S_2 and S_3 data, and measurement and subtraction of the background noise level of the total power image. Near the subradar point, the minimum total error is about 0.02, at an incidence angle of 45° the error in m_l is 0.04, and at an incidence angle of 70° the error is around 0.06. Sources of error in the m_l values are discussed further by *Carter et al.* [2004].

3. Interpreting Degree of Linear Polarization Data: Examples From AIRSAR

[13] The value of the degree of linear polarization (m_l) depends on the physical properties of the surface, the radar viewing geometry and the amount of spatial averaging [*Stacy*, 1993; *Carter et al.*, 2004]. For a circularly polarized incident wave, linear polarization is produced when the V component of the wave is preferentially transmitted into the surface. The value of m_l therefore depends on the Fresnel power transmission coefficients [*Jackson*, 1999],

$$T_H(\theta,\epsilon') = \frac{4\cos\theta\sqrt{\epsilon' - \sin^2\theta}}{\left(\cos\theta + \sqrt{\epsilon' - \sin^2\theta}\right)^2} \tag{4}$$

$$T_V(\theta,\epsilon') = \frac{4\epsilon'\cos\theta\sqrt{\epsilon' - \sin^2\theta}}{\left(\epsilon'\cos\theta + \sqrt{\epsilon' - \sin^2\theta}\right)^2}, \tag{5}$$

where θ is the incidence angle and ϵ' is the real part of the dielectric constant ($\epsilon = \epsilon' + i\epsilon''$). At normal incidence, $T_H = T_V$ and the degree of linear polarization is zero. As the incidence angle increases, the difference between the transmission coefficients increases, as does the degree of linear polarization. Higher surface dielectric constants will produce higher m_l values. Loss in the surface medium will decrease the subsurface radar echo relative to the surface echo power, producing a lower m_l value. The loss tangent of Venus surface materials is not known, but assuming dry-rock values of 0.001–0.01 [*Campbell and Ulrichs*, 1969], the 12.6-cm radar wave is most likely penetrating a few centimeters to ~1 m into the surface. Spatial averaging over an area containing mantled and nonmantled surfaces will result in an m_l value lower than that expected for a fully mantled area. The large number of variables that contribute to m_l make it impossible to extract numerical values for the dielectric constant or depth of mantling layers. However, it is still possible to infer penetration of the radar wave into the surface and use this to investigate changes in surface properties across a region.

[14] Terrestrial radar data provide a good demonstration of this technique. The NASA/JPL AIRSAR system records the full Stokes scattering matrix and can therefore be used to generate degree of linear polarization (m_l) maps as well as ratios of the backscattered power in the HH and VV polarizations. The first letter in the HH (or VV) designation refers to the transmitted polarization direction while the second refers to the received polarization. In AIRSAR data, high m_l values typically correspond to surfaces that are smooth at radar wavelengths. For example, AIRSAR data of Death Valley show that sand mantled areas that are smooth at wavelength scales exhibit enhanced linear polarization and decreased σ_{HH}/σ_{VV} ratios [*Carter et al.*, 2004].

[15] Another particularly good example occurs near a small cinder cone northeast of Sunset Crater Volcano in Arizona. Figure 1 shows a radar dark deposit to the north of the cone that produces m_l values of around 30% at L-Band (24 cm). The σ_{HH}/σ_{VV} ratio in that same area is about 0.6, consistent with preferential transmission of V-polarized waves through the surface-atmosphere interface. In Figure 1c, the polarization angle changes as the plane of incidence and reflection for the sides of the cone tilts in the azimuth direction. The radar dark region is covered in welded cinders with fine-grained ash filling in to produce a fairly uniform surface. Short grasses grow in patches on the deposit, but there are few trees or shrubs that would produce a strong reflection at 24 cm wavelength.

[16] Although high m_l values are usually associated with smooth deposits of unconsolidated debris, it is also possible for the radar to penetrate into solid surfaces. For example, AIRSAR P-Band (68 cm) data show penetration effects for some smooth lava flows on Kilauea. These flows formed when lava cooled in topographic depressions; nearby pahoehoe flows that traveled downhill are considerably rougher [*Campbell and Shepard*, 1996]. Figure 2 shows an image of the Kilauea caldera along with the corresponding degree of linear polarization overlay. Areas of smooth ponded lava flows are marked on the radar image. The degree of linear polarization over the ponded flows is ~0.30, and it appears that in these limited areas the radar wave is able to penetrate the surface and reflect from air gaps within the flow.

[17] These terrestrial examples demonstrate that high m_l values can be generated from a range of surface types, including deep fine-grained and coarse (volume scattering) material, smooth surfaces with embedded scatterers, and smooth lava flows with internal reflectors. These scenarios are illustrated in Figure 3, and represent possible analogies to surfaces on Venus that have a linearly polarized echo component.

[18] Not all mantled surfaces will produce a measurable linear polarization signature, and areas that show morphological evidence of mantling (e.g., impact crater deposits, windstreaks) in Magellan data do not always correspond to high m_l values in the Arecibo data. Sketches of such

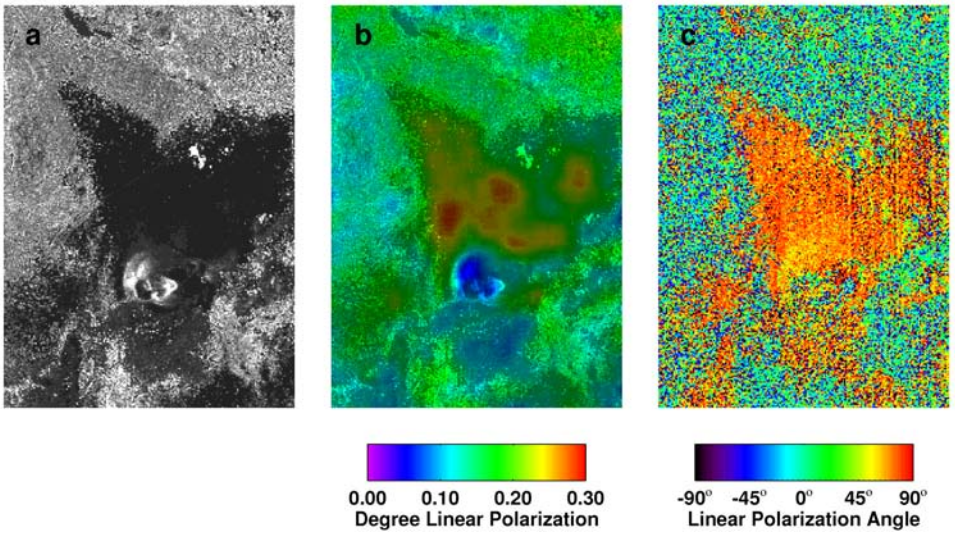

Figure 1. AIRSAR L-Band (24 cm) images of a cinder cone near Sunset Crater in Arizona. The vertical dimension of the image is ~5 km. Range increases to the right; the incidence angle of the cinder cone is about 60°. (a) Total power image showing a radar dark deposit. (b) The degree of linear polarization stretched to a color scale and overlaid on the total power image. (c) The linear polarization angle. Notice that the angles change as the slopes on the side of the cinder cone tilt in the azimuth (Doppler) direction.

scenarios are shown in Figure 4. If a surface layer is too deep, too lossy, or has too few subsurface reflectors, the radar wave will attenuate significantly and will have negligible linear polarization. Similarly, a gradual change in dielectric constant will not provide a reflecting surface capable of producing a linearly polarized echo. Surfaces that are rough at wavelength scales will randomize the polarization state of the wave, again producing no linear polarization.

4. Radar Polarimetry of Volcanic Deposits on Venus

[19] The degree of linear polarization maps of Venus show numerous features, which typically have m_l values between 0.1 and 0.35, and which stand out as having higher m_l values from the surrounding plains. Some of these features correspond to impact crater deposits as discussed by *Carter et al.* [2004]. We also observe a significant degree of linear polarization associated with some volcanic deposits on Venus, and we interpret the high m_l values as evidence of subsurface scattering of the incident radar wave. As discussed in section 3, the large number of variables that can alter the value of m_l make it impossible to quantitatively derive surface parameters such as the depth and dielectric constant of surficial layers. However, the polarimetry results can still be used qualitatively to search for mantling deposits and lava flows with unusual properties.

[20] The examples discussed in this paper were chosen because the spatial extent of linear polarization enhancements are closely matched with volcanic features visible in Magellan and Arecibo images. They represent the clearest associations between volcanic areas and m_l values consistent with subsurface scattering in the Arecibo polarimetry. Our goal was to investigate areas where this clear correspondence occurred and discuss what the enhanced m_l values reveal about the different geologic settings.

[21] The Arecibo degree of linear polarization maps can be compared to the higher-resolution Magellan SAR imagery, as well as Magellan altimetry and radiometry data, to investigate the geologic context of the inferred subsurface scattering. To assist in the analysis, overlays were created by stretching the degree of linear polarization data to a color scale and combining them with Magellan image data for the same area (Figures 5–10). The Arecibo data registers with the Magellan data to within a few kilometers, or less than a pixel in the spatially averaged data. The degree of linear polarization data were smoothed during the overlay process, so their spatial resolution has been reduced by a factor of 3 to 5 from the values given in section 2. The color stretch was optimized for each overlay.

[22] The overlays show that m_l varies across individual features, and the maximum value of the degree of linear polarization changes from feature to feature. All of the variables discussed in section 3 could be responsible for changes in m_l across individual features. However, it seems most likely that changes in the depth of the mantling deposit, changes in the presence or distribution of subsurface scatterers, or the fraction of each pixel covered in penetrable material, is the cause of the m_l variation across a given feature. The volcanic features associated with enhanced linear polarization can be divided roughly into three groups: plains region volcanic fields, lava flows, and highland volcanoes.

4.1. Plains Region Volcanic Fields

[23] Clusters of small (several kilometers in diameter) shield volcanoes are ubiquitous on the volcanic lowland plains, and some of the larger fields visible with Arecibo are correlated with an enhanced degree of linear polarization. Examples of two such areas are shown in Figures 5 and 6. The degree of linear polarization is usually greatest in the immediate vicinity of the volcanoes and drops to very low values (blue) on the surrounding plains. For these dome

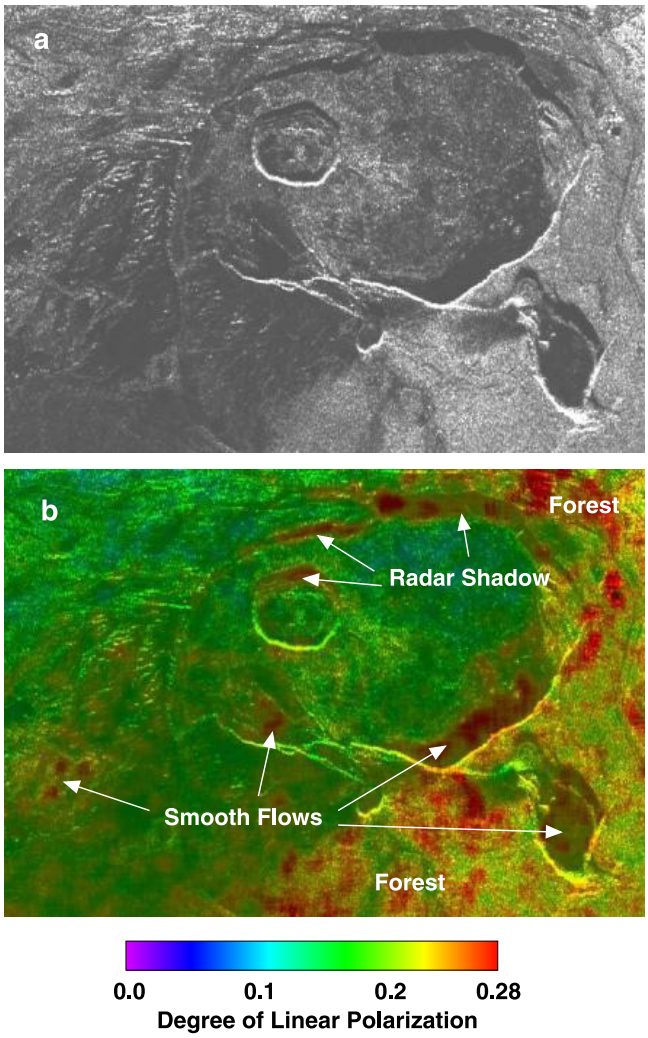

Figure 2. Enhanced linear polarization correlated with smooth, radar-dark flows on Kilauea. (a) AIRSAR P-Band (68 cm) image of the summit of Kilauea. Range increases from the top of the image to the bottom; the incidence angles range from 22° to 48°. The horizontal image dimension is 5.3 km. The radar bright regions to the right and lower right are forested. (b) The degree of linear polarization stretched to a color scale and overlaid on the total power image. Locations of smooth flow areas are marked, along with areas of radar shadow and forest.

fields, high m_l values overlap complex flow patterns where the radar cross-section changes over spatial scales much smaller than the pixel size of the Arecibo polarimetry data.

[24] Figure 5 shows volcanic fields in the vicinity of West crater. A field in the lower right portion of the image (marked A) provides a good example of how the linear polarization enhancement is often restricted to a localized area around a specific shield field. In the north and central parts of the image, high m_l values are associated with small volcanoes and lava flows. Aeolian processes have been active in this area as well. In the northwest part of the image, marked B, m_l values of about 0.15 correspond to an area of windstreaks. The windstreaks start at the base of a bright, east-west trending ridge and fan out to the southwest. In the southwest portion of the figure, there is an area of enhanced linear polarization which ends abruptly at the base of an elevated deformation belt (marked C); this may be an area where wind-blown material is trapped against a topographic high. In areas of windstreaks, mantling of a smooth, solid-rock surface by unconsolidated material (Figure 3a) may explain the linear polarization observed.

[25] Figure 6 shows a shield field at 22°N and 332°E (near the crater Aurelia) that was cited as a possible site of pyroclastic deposits early in the Magellan mission [*Head et al.*, 1991; *Guest et al.*, 1992]. Individual shield volcanoes have concentric regions of low radar return that brighten (to the level of the surrounding plains) with distance from the volcanic center. Radar bright, triangular patches south of a few of the shields have been interpreted as wind-scoured areas, and dark margins around the bright triangles suggest that material piles up at the edges of the scoured regions [*Guest et al.*, 1992]. This shield field has m_l values of up to 0.16, which is evidence that there is likely smooth, fine-grained debris in this area. The shields lie within the Aurelia parabola, which is also associated with high m_l values [*Carter et al.*, 2004], and so mantling material in the area may have been generated by the Aurelia impact. Regardless of how the mantling deposit was formed, it is likely that the high m_l values are generated by a scenario similar to those shown in Figure 3a or 3b.

4.2. Lava Flow Complexes

[26] In a couple cases, enhanced linear polarization corresponds to lava flow complexes. Figure 7 shows a volcanic field in Guinevere Planitia at 17.5°N, 313°E. The highest m_l values are associated with a series of flows with a mixture of radar bright and radar dark regions, and emissivity values

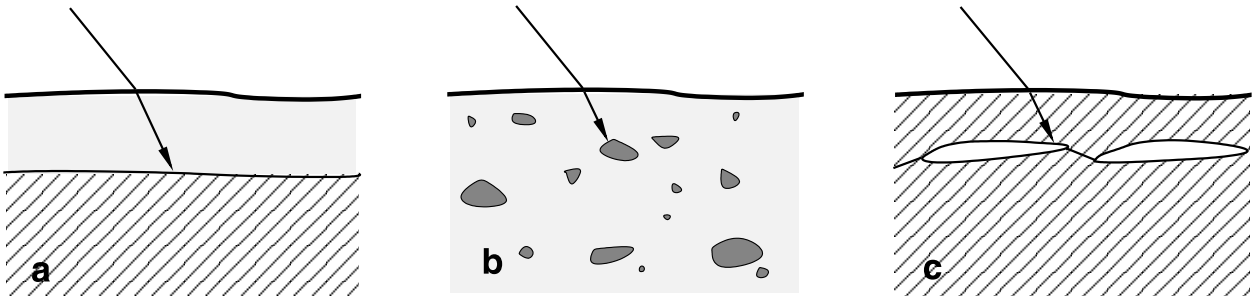

Figure 3. A sketch of three subsurface interfaces capable of producing a linearly polarized radar echo. (a) Scattering from a subsurface layer. (b) Penetration into a smooth mantled surface with buried scatterers. (c) Scattering from subsurface discontinuities in lava flows.

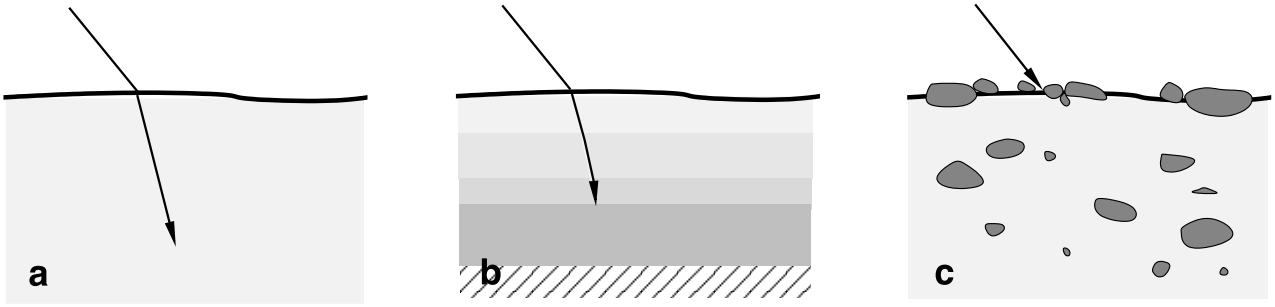

Figure 4. Illustration of mantled surfaces that will not produce a linearly polarized radar echo, even if the wave is able to penetrate into the surface. (a) Surface material is lossy or layer is deep (several meters). (b) Gradual change in dielectric constant with depth (c) Surface that is rough at wavelength scales.

ranging from 0.80 to 0.84 (plains average emissivity). Lava flows on the western flank of Sif Mons (Figure 8) also show enhanced linear polarization. The high m_l values are associated with areas of high and low backscatter cross section values, but most of the linear polarization feature is associated with a darker complex of flows that begin near the central caldera and extend onto the plains. The emissivity values over the flows are only slightly below the plains

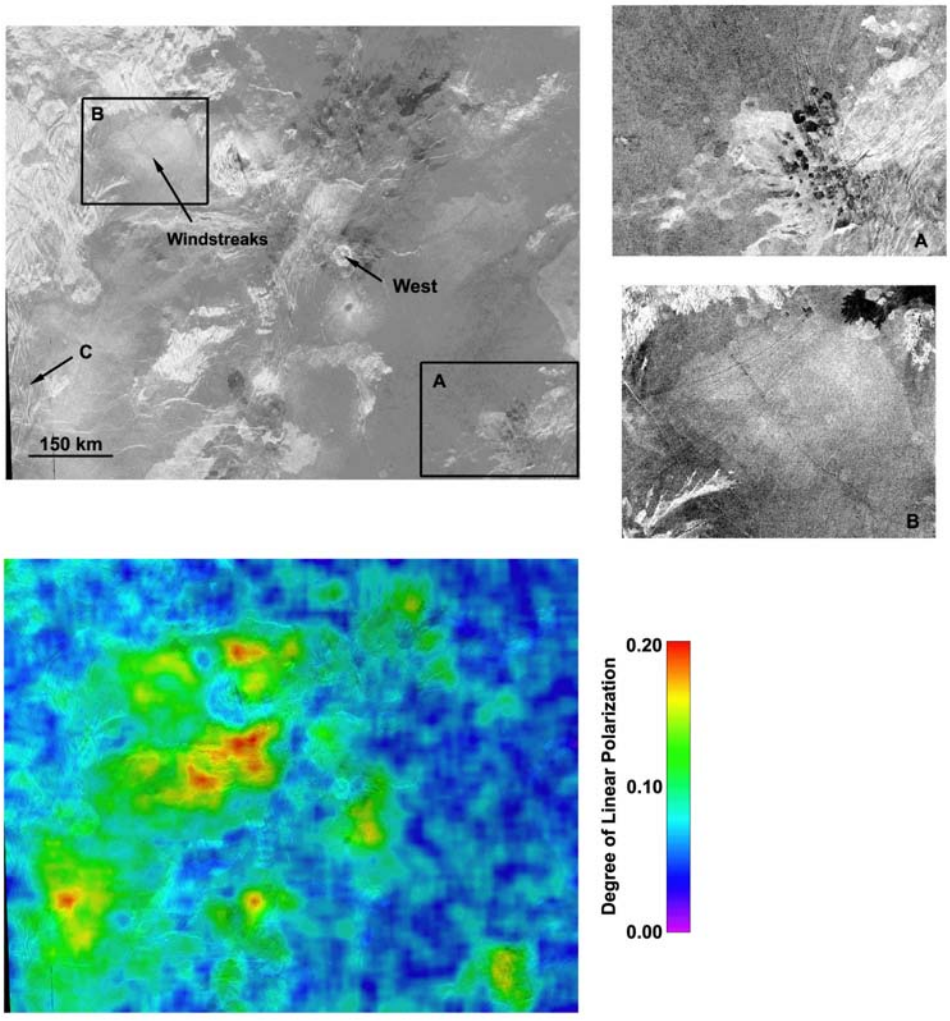

Figure 5. Volcanic fields and windstreaks in the vicinity of West crater. The top left image is a Magellan SAR image, and the corresponding degree of linear polarization overlay is shown below. Regions A, B, and C are discussed in the text, and higher-resolution Magellan images of areas A and B are shown in the right column.

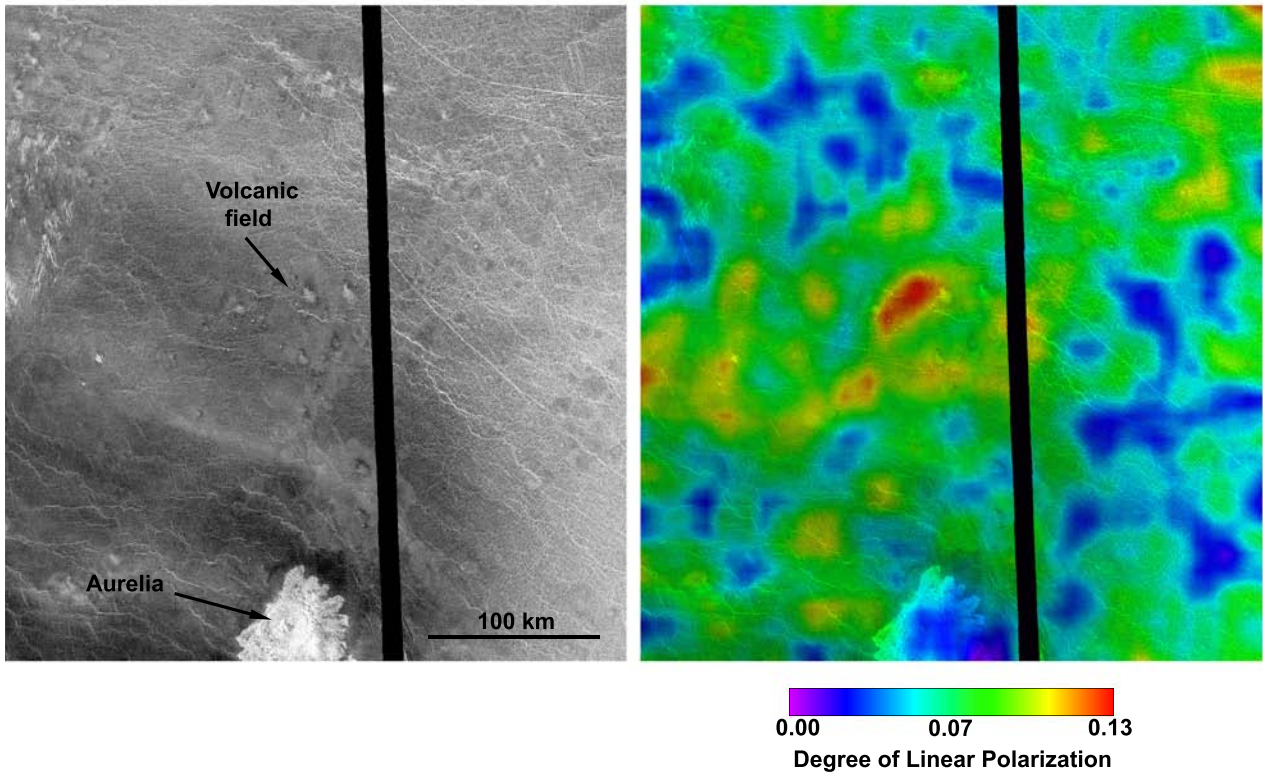

Figure 6. Volcanic field with windstreaks, located north of Aurelia crater. The degree of linear polarization overlay is on the right, and the Magellan SAR image is shown on the left for comparison.

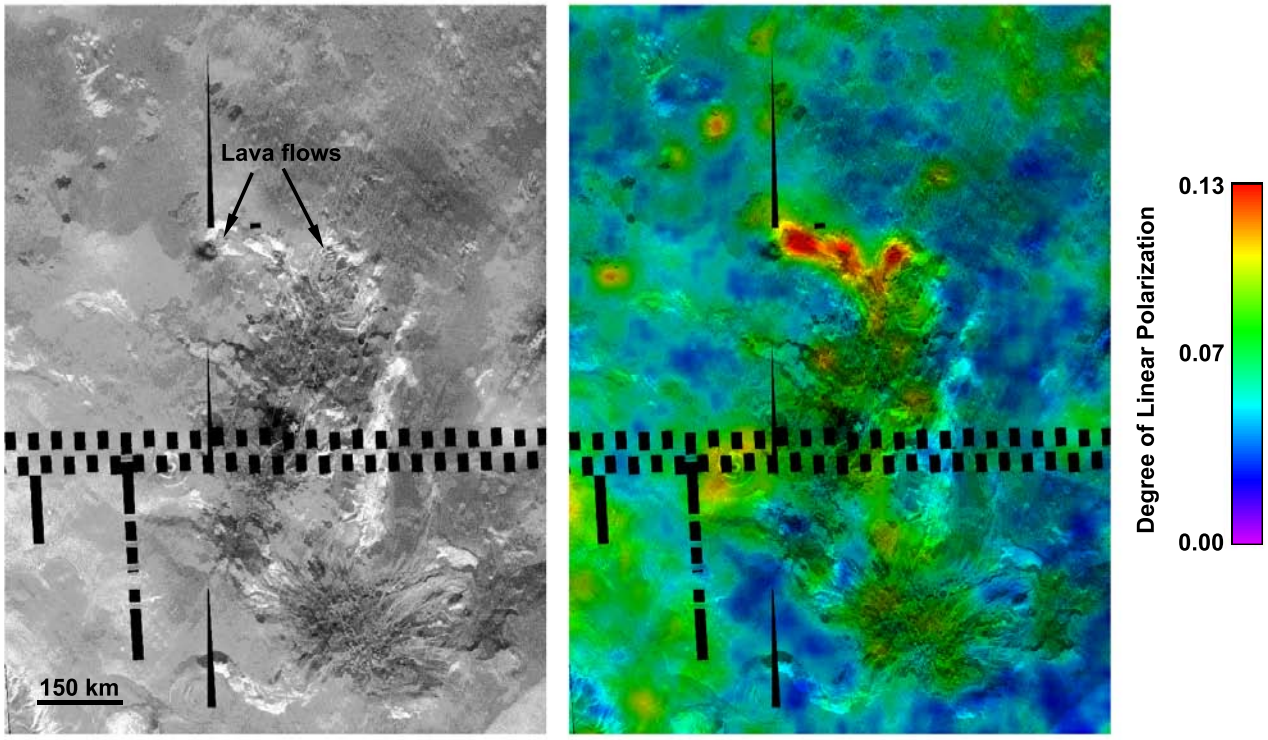

Figure 7. Volcanic field in Guinevere Planitia at 17.5°N, 313°E. The degree of linear polarization overlay is on the right; a Magellan SAR image is shown on the left for comparison. High m_l values correspond to a flow with radar bright and dark sections in the Magellan SAR imagery.

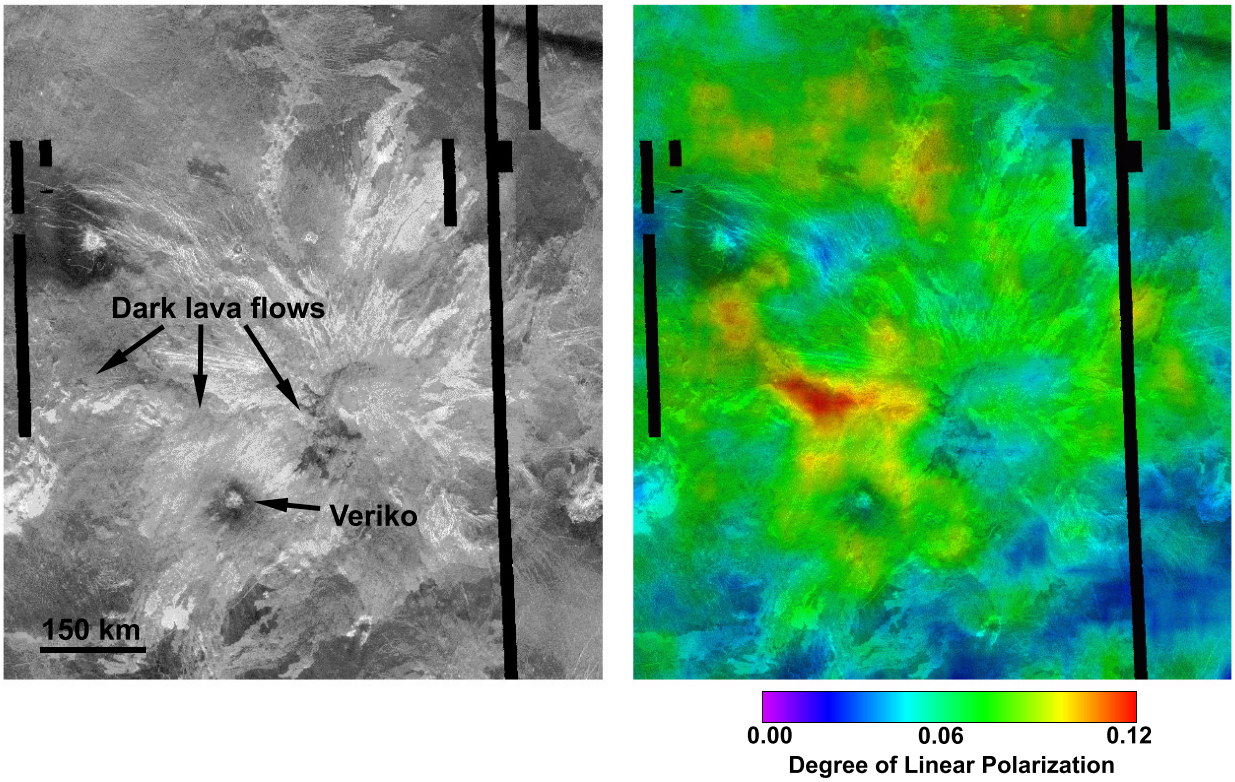

Figure 8. Radar dark lava flows on the flank of Sif Mons show enhanced linear polarization. The degree of linear polarization overlay is on the right; a Magellan SAR image is shown on the left for comparison.

average, ranging from 0.80 to 0.83. The crater Veriko, located on the southwest flank of Sif, is surrounded by areas of enhanced polarization [*Carter et al.*, 2004]. The m_l values are lower than those associated with the flows, form a partial ring around the crater, and may be due to penetration of the radar wave into an impact generated deposit.

[27] It is interesting that the polarimetry data highlight specific lava flow complexes as having different physical properties from other flows on Venus of similar backscatter and emissivity. Given the difficulty in creating pyroclastic deposits on Venus, and the lack of corresponding high emissivity values, it seems unlikely that the radar wave is refracting into ash deposits. Perhaps in these cases the radar is able to penetrate into the surface of the lava and reflect from air gaps (Figure 3c), as was shown to occur at Kilauea (Figure 2). Air gaps between thin superposed flows could produce dielectric discontinuities in the lava that would act as radar reflectors. The AIRSAR radar data for Kilauea were taken at a wavelength of 68 cm, which will have greater penetration depth in solid material than the 12.6-cm wavelength wave used in the Arecibo Venus observations. Air gaps in the Venus flows have to be within tens of centimeters of the surface to provide a measurable subsurface reflection, assuming loss tangents of ~0.01.

4.3. Highland Volcanoes

[28] At high elevations, many mountains on Venus show a dramatic increase in Fresnel reflectivity and a corresponding decrease in emissivity. Most of the highland regions with altitudes large enough to show this change are near the equator, where the emissivity drops for altitudes that are ~3 km above the mean radius, and returns to normal values at about 4.2 km elevation [*Arvidson et al.*, 1994]. For Maxwell Montes, at a latitude of 65°, the change in radar properties occurs at about 5 km above mean radius. The onset of high reflectivity at specific altitudes suggests that a temperature- and/or pressure-dependent process is responsible for the changes; for example, alteration of a mineral phase or condensation of conducting or semiconducting atmospheric constituents. Emissivities as low as 0.3 have been measured over highland regions, and since there is no water on Venus, these low values require an unusual geologic material [*Schaefer and Fegley*, 2004; *Pettengill et al.*, 1996]. The low emissivities have also been attributed to volume scattering in a low loss medium [*Tryka and Muhleman*, 1992], but this model requires a nearly lossless matrix material.

[29] Arecibo images include the highland volcanoes Theia Mons, Gula Mons and Tepev Mons, all of which show the emissivity change with altitude. Gula Mons shows no linear polarization enhancement, but the volcanoes Theia and Tepev Montes (Figures 9 and 10) both show high m_l values associated with high-altitude summit areas. Maat Mons, which has altitudes up to 9 km but does not display the low-emissivity behavior, is not visible in the Arecibo data.

[30] Figure 9 shows portions of the low-emissivity flows on the summit of Theia Mons that show enhanced linear polarization. The highest m_l values (0.24) correspond to

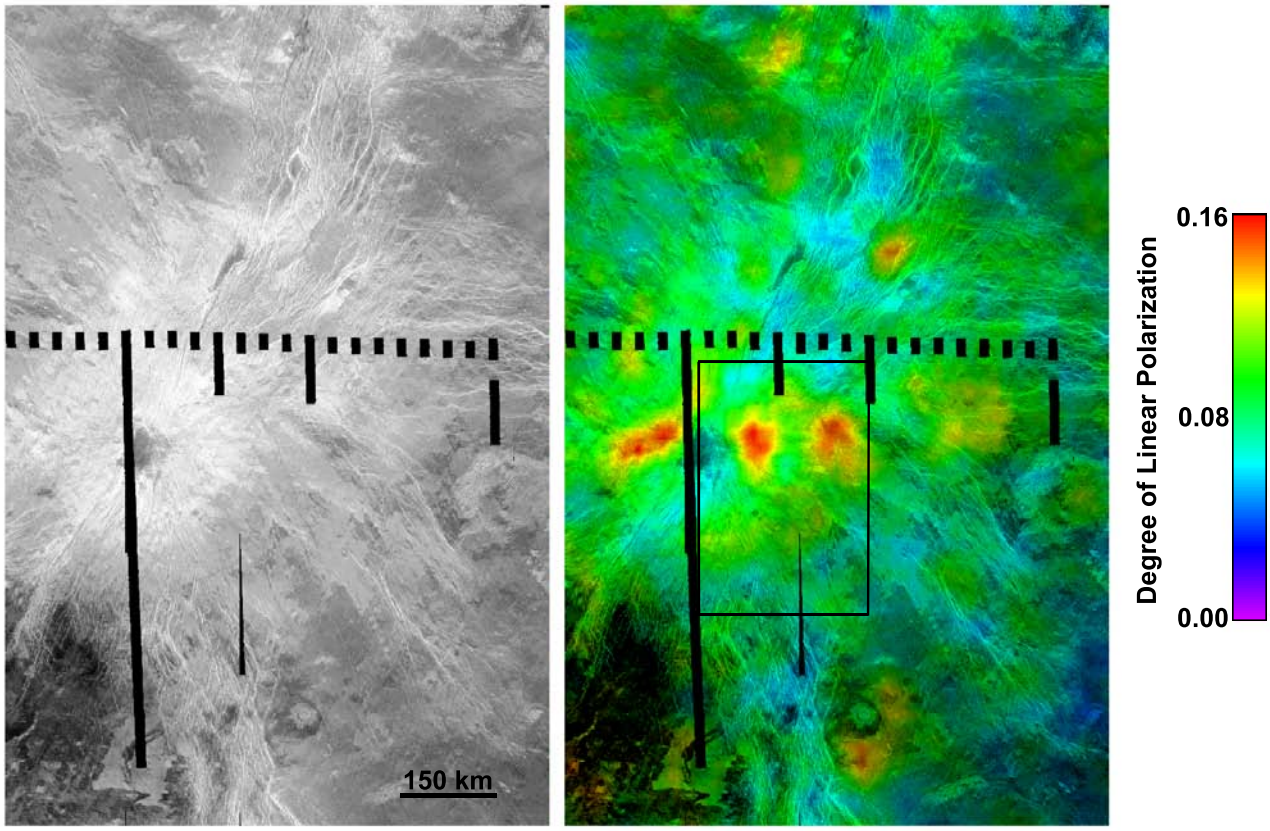

Figure 9. Theia Mons is one of two highland volcanoes that show enhanced linear polarization from summit areas. The degree of linear polarization image is on the right and the corresponding Magellan SAR image is on the left. The box on the degree of linear polarization image marks the boundaries of the image in Figure 11.

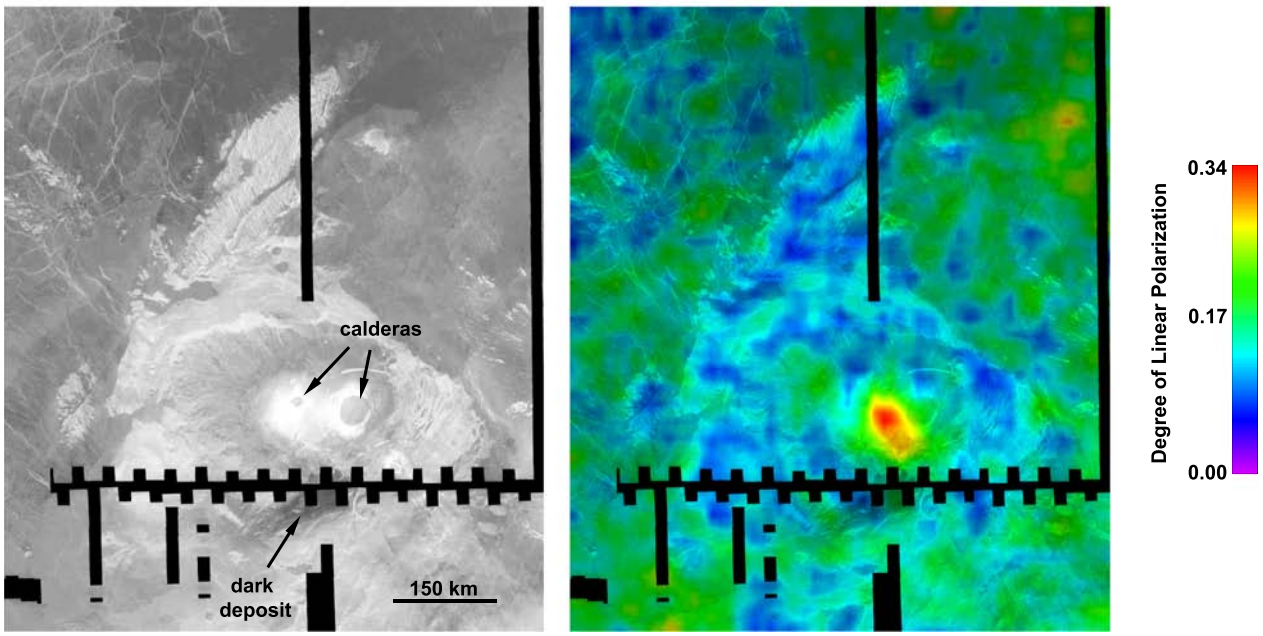

Figure 10. Degree of (left) linear polarization overlay and (right) Magellan SAR image showing high m_l values near the summit of Tepev Mons. The location of the radar dark deposit thought to be pyroclastic material [*Campbell*, 1994] is marked on the SAR image.

Table 2. Magellan HH/VV Ratios Over Theia Mons

Box	Number of Pixels	HH[a]	VV[a]	HH/VV[a]
A	1598	0.13 ± 0.03	0.15 ± 0.04	0.87 ± 0.31
B	3234	0.12 ± 0.03	0.11 ± 0.02	0.96 ± 0.30
C	897	0.11 ± 0.03	0.11 ± 0.03	1.0 ± 0.38
D	1224	0.21 ± 0.06	0.22 ± 0.04	0.95 ± 0.34
E	1044	0.21 ± 0.08	0.29 ± 0.08	0.72 ± 0.34
F	780	0.23 ± 0.08	0.30 ± 0.08	0.77 ± 0.33
G	832	0.39 ± 0.12	0.41 ± 0.09	0.95 ± 0.36
H	1960	0.27 ± 0.09	0.37 ± 0.08	0.73 ± 0.29
I	1312	0.17 ± 0.05	0.19 ± 0.05	0.89 ± 0.39
J	221	0.25 ± 0.07	0.39 ± 0.08	0.64 ± 0.22
K	380	0.21 ± 0.06	0.32 ± 0.07	0.66 ± 0.24
L	1054	0.44 ± 0.13	0.52 ± 0.10	0.85 ± 0.30
M	754	0.42 ± 0.12	0.49 ± 0.09	0.86 ± 0.29
N	1036	0.28 ± 0.08	0.38 ± 0.08	0.74 ± 0.26

[a]Plus/minus values are 1 standard deviation of the average.

areas where the emissivity values drop to 0.35. On the eastern flank of Theia, the emissivity rises to 0.55 and the degree of linear polarization declines to 0.20. The high m_l values on Theia are associated with flows that exhibit complex variation in radar backscatter and it is not obvious from the SAR images why some areas show enhanced linear polarization while others do not.

[31] This area to the east of the summit is one of the places where the Magellan spacecraft acquired V-polarization data, making it possible to compare Magellan σ_{HH}/σ_{VV} ratios with our degree of linear polarization measurements. *Plaut* [1993] noted that low σ_{HH}/σ_{VV} ratios occur over parts of the summit and that there are 1- to 2-dB variations in the σ_{HH}/σ_{VV} ratios of different lava flows. In a few cases, areas tens of kilometers in size are darker than their surroundings in the σ_{HH} image, but are uniformly bright, and indistinguishable from surrounding terrain, in the σ_{VV} image. Table 2 shows average σ_{HH} power, σ_{VV} power and σ_{HH}/σ_{VV} values, and their standard deviations, for boxes across Theia Mons. The locations of the boxes are shown in Figure 11. Box locations were limited to the central portion of the σ_{VV} data strips to avoid potential calibration problems. The high m_l values correspond to flows with σ_{HH}/σ_{VV} ratios as low as 0.64 (box J), although the σ_{HH}/σ_{VV} ratio changes on small (10 km) spatial scales and the high m_l area also overlaps flows with higher ($\sim$1) σ_{HH}/σ_{VV} ratios. Areas to the southeast of the Theia Mons summit, where the degree of linear polarization is significantly lower, have σ_{HH}/σ_{VV} ratios of $\sim$1, as is typical for rough surfaces [*Campbell et al.*, 2004]. There is significant scatter in pixels measured for each box and the standard deviations on the measurements are fairly large. However, in some places (e.g., boxes J and K) these values are consistent with subsurface scattering.

[32] Measured σ_{HH}/σ_{VV} ratios can be used to estimate a degree of linear polarization. *Campbell et al.* [2004] derive an expression for the degree of linear polarization as a function of backscatter cross sections for the HH, VV, and HV polarizations. The σ_{HV}/σ_{VV} ratio reaches a maximum of about 1/3 for very rough surfaces [*Campbell et al.*, 2004], and using σ_{HV}/σ_{VV} ranging from 0 to 1/3 results in expressions bounding the degree of linear polarization. Measured σ_{HH}/σ_{VV} values of 0.64 are consistent with degree of linear polarization values between 0.27 and 0.35, which are somewhat larger than the measured m_l values of 0.20. The Arecibo polarimetry data has a much larger pixel size, so it is not surprising that the m_l values in Figure 7 are smaller than this predicted range.

[33] Tepev Mons, shown in Figure 10, also has a high-reflectivity summit region, with two large calderas that may contain fine-grained ash or dust [*Campbell and Rogers*, 1994]. The highest m_l values occur in a topographic "saddle" between the two calderas that is characterized by Fresnel reflectivity slightly lower than the average across the summit region. The dark, low dielectric constant mantling deposit [*Campbell and Rogers*, 1994] does not show any linear polarization signature, nor does the large, eastern caldera that is thought to be filled with fine debris.

[34] The relationship between the degree of linear polarization values and the very low emissivity mountaintops is unexpected. As discussed above, these low emissivity values are thought to be indicative of a high dielectric constant semiconducting or conducting material, not a low dielectric mantling layer. Penetration into high dielectric surfaces will produce a larger degree of linear polarization, but a high ϵ' value can also increase the surface echo from areas of rough terrain and thereby reduce the signature of any subsurface echo component.

[35] For a very restricted range of surface roughness values, it is also possible for surface-only scattering to

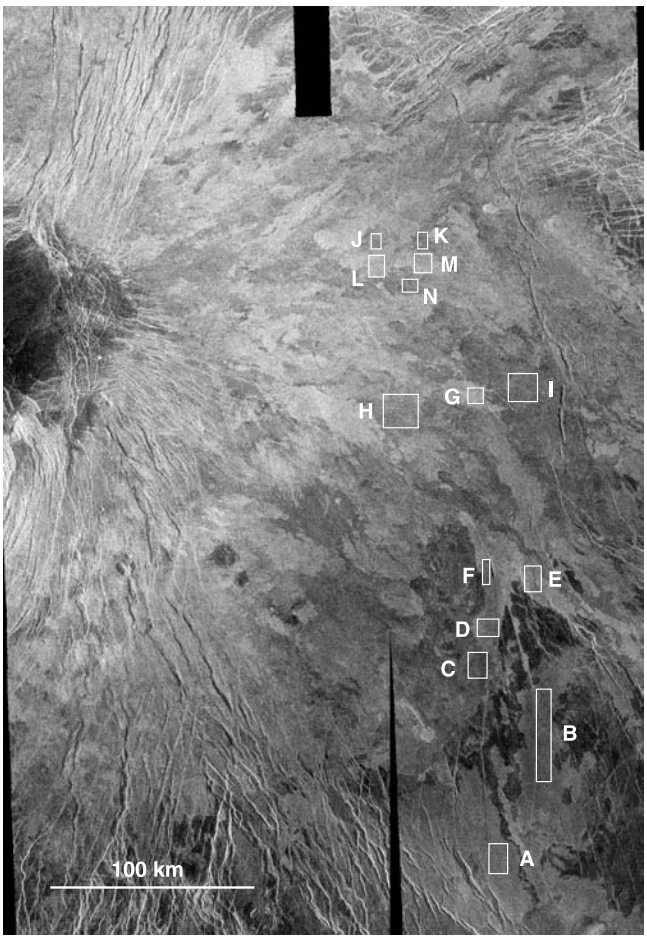

Figure 11. Magellan SAR image of Theia Mons (H-polarized), showing the locations of boxes where the HH/VV ratios shown in Table 2 were measured.

generate an enhanced degree of linear polarization. Surfaces with an rms height less than $\lambda/20$ can be described using the small perturbation model (SPM), which predicts that surface scattering can generate $\sigma_{HH}/\sigma_{VV} < 1$. Figure 12 shows σ_{HH}/σ_{VV} ratios which are solely a function of ϵ' and θ in the first-order small perturbation model [*Barrick and Peake*, 1967; *Campbell et al.*, 2004]. The right axis shows corresponding m_l values that were computed by assuming $\sigma_{HV} = 0$. The model is shown for a range of incidence angles. Small perturbation scattering is clearly capable of producing very high m_l values. However, this model is only valid in areas where the surface roughness is less than ~0.6 cm on horizontal scales of 12.6 cm. Measurements for Hawaiian lava flows [e.g., *Campbell and Shepard*, 1996; *Shepard et al.*, 2001; *Campbell et al.*, 2004] show that the σ_{HH}/σ_{VV} ratio trends towards unity as the roughness approaches this limit. For the SPM to explain the enhanced m_l values, the surface of the lava flows would have to maintain a roughness of tens of millimeters over areas large enough to contribute significantly to the power measured on spatial scales of 150 m (for Magellan) or 12 km (for Arecibo). It is unlikely that these roughness conditions would be satisfied over such large areas.

[36] Despite the difficulties with both the subsurface and surface scattering scenarios described above, it is clear that some of the low-emissivity areas are conducive to producing a linearly polarized echo. For both the SPM case and the subsurface scattering model, surfaces in the high m_l areas must be very smooth at wavelength scales. The VV polarization Magellan data across Theia Mons provide independent confirmation of the values measured with the Arecibo polarimetry. Interpretation of the scattering in summit areas remains uncertain, but perhaps the radar wave is able to penetrate into high dielectric material in limited cases of very smooth surface texture.

5. Conclusions

[37] Arecibo degree of linear polarization maps show high m_l values associated with some volcanic fields, lava flows, and highland volcanoes. In some cases, such as the volcanic field near the crater Aurelia (Figure 6), the linear polarization signature is most likely generated by scattering from within a mantling layer or from a buried rough interface. This shield field is also the only area previously considered as a potential pyroclastic deposit, within the Arecibo coverage, that is correlated with a high degree of linear polarization. Areas of windstreaks are found in close proximity to some volcanic fields; these areas are most likely covered in fine debris with a depth of a few centimeters to ~1 m.

[38] In a couple of cases, the radar polarimetry data "selects" lava flow complexes as having different physical properties from flows with similar radar backscatter. Neither of the high m_l flows has a high emissivity that would suggest a deposit of fine-grained mantling material. These may be cases where the radar wave is able to penetrate into the lava and reflect from discontinuities within a layered flow complex. The linear polarization data also highlight specific regions on the low-emissivity summits of Theia and Tepev Montes as allowing significant refraction and subsurface scattering. Given the high dielectric constant materials thought to be present on these surfaces [*Pettengill et al.*, 1996], the high m_l values in these areas may be generated by shallow penetration into a very smooth, high dielectric material. The low dielectric constant areas on the summit of Tepev Mons [*Campbell*, 1994] do not show a linearly polarized echo component; perhaps they are too thick, or lack embedded rocks capable of returning a significant radar echo. It is interesting that the summits of Theia and Tepev Montes show high degree of linear polarization values, but other high-altitude, low-emissivity areas, such as Gula Mons, are not associated with an enhanced linear polarization signature. Summit areas on Gula Mons may be too rough at wavelength scales to produce a measurable degree of linear polarization.

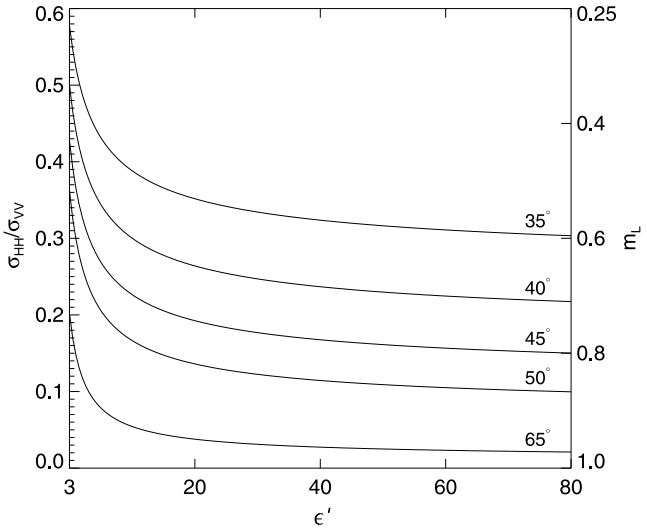

Figure 12. The σ_{HH}/σ_{VV} ratio predicted by the first-order small perturbation model for four different incidence angles and a range of dielectric constants, ϵ'. Degree of linear polarization (m_l) values were computed for the σ_{HH}/σ_{VV} axis by assuming that σ_{HV}/σ_{VV} is 0.

[39] Future radar observations at 70 cm wavelength may help constrain the scattering mechanisms that produce the linearly polarized echoes. The longer wavelength will be able to propagate farther into the surface, and could potentially return linearly polarized echoes from buried structures that are invisible to the 12.6-cm radar. Higher resolution radar polarimetry, for example dual-polarization images provided by an orbital spacecraft, would also allow for more detailed modeling of the surface properties. The highest m_l values observed in the Arecibo data are associated with impact craters [*Carter et al.*, 2004] and with the volcanic features discussed above, but wide areas of the plains show m_l values that are slightly greater than the expected noise background level [*Carter et al.*, 2004; *Carter*, 2005]. Unfortunately, the limited latitude/longitude extent of the Arecibo data, uncertainties in the dielectric properties of the surface, and the unknown aerial extent of deposits within each 12- to 16-km spatial pixel prevent a quantitative analysis of the fraction of the Venus surface covered in fine material. At high resolution (tens of meters per pixel), it is more reasonable to assume that the surface is uniform across a single pixel. With this assumption, it becomes feasible to explore different scattering models, to

model the corresponding dielectric constants, and to study the spatial distribution of any inferred surface deposits.

Appendix A: Calibrating Linear Polarization Angles in Arecibo Data

[40] In order to measure the direction of the linear polarization vector relative to the plane of incidence and reflection, it is necessary to calibrate the linear polarization angles (χ). Every resolution cell with a linear echo power component also has an associated linear vector direction that is measured on the plane of the sky by the Arecibo telescope. To find a value for χ that can be compared to what is expected from surface scattering models, the measured polarization angles must be corrected for the parallactic angle produced by the field-of-view rotation during telescope tracking (χ_{pa}) and referenced to an absolute plane-of-sky angle using a calibrator source with a known polarization direction.

[41] The parallactic angle was corrected during the initial range processing (decoding) of the data. Without this correction, the direction of the linear polarization vector for a given resolution element changes as the telescope tracks, and when data are averaged over the course of a day the linear polarization vectors do not combine correctly. The rotation was performed using an expression based on the zenith angle (z), azimuth (A), and telescope latitude (Λ) [*Rankin et al.*, 1972],

$$\tan \chi_{pa} = \frac{\sin A}{\cos A \cos z - \tan \Lambda \sin z}. \quad \text{(A1)}$$

This formula was used to rotate the polarization angles for all the runs to what they would be at transit (where the azimuth equals zero).

[42] As the received signals propagate through a given path length, the linear polarization angle changes, and this instrumental angle χ_0 must be accounted for. We used a spinning dipole, located just above the primary reflector of the 305-m telescope and radiating a pure 2.38-GHz signal, to calibrate the polarization angles. This calibration dipole produces a data dropout every time it is aligned north-south, making it possible to link the plane-of-sky direction of the polarization angle with the angle measured by the receiving system. We took about 1 min of dual-polarization radar data on the calibration dipole while the telescope was pointed to 0° azimuth, and used these data to compute the polarization angle (χ_0) measured by the radar when the dipole is oriented north-south. The polarization angles measured for Venus were rotated by χ_0, so that the north plane-of-sky direction at 0° azimuth would correspond to a polarization angle of zero degrees.

[43] It is possible to determine what the polarization angles (measured around the subradar point on the plane of the sky) should be if the linearly polarized echoes are produced by subsurface scattering. If the linear polarization is generated by preferential transmission of the V-polarized component of the wave into the surface, χ will be parallel to the local plane of incidence. Therefore, if a surface feature with a linear-polarized echo component has a position angle on the sky 30° away from north, the predicted polarization angle is also 30°. The position angles of eight linear polarization features on Venus were measured with respect to plane-of-sky north, and compared with an average value of the corresponding measured, calibrated polarization angle. If the linearly polarized echoes are generated by subsurface scattering, the two angles will be the same. If the linear polarization is produced by multiple-bounce mechanisms, then the measured polarization angles will be rotated 90° from the local plane of incidence. (In practice, the positions of the features were measured with respect to the Doppler axis of Venus, and ephemeris data were used to determine the position of the Doppler axis with respect to plane-of-sky north.) Figure A1 shows a plot comparing the measured and predicted polarization angles, and shows that the measured polarization angles approximate what is expected from subsurface scattering, although they appear to have a small systematic offset. This could be accounted for by the error in determining the exact moment that the dipole was oriented north-south.

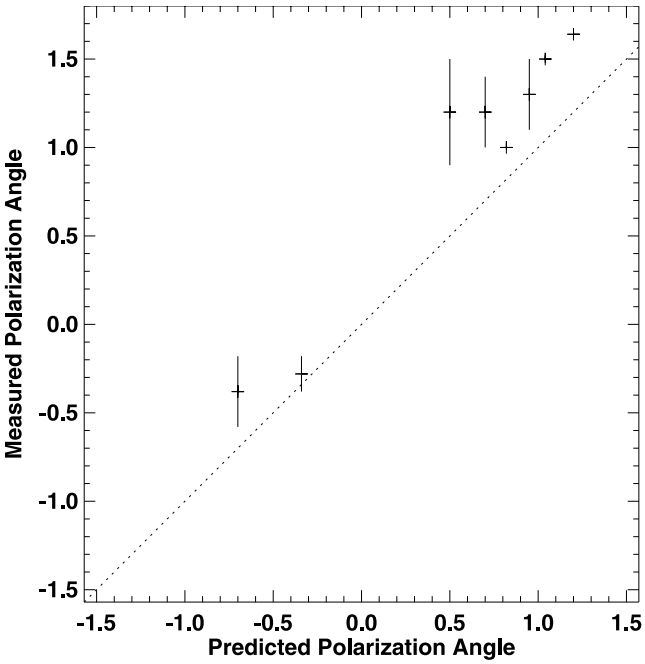

Figure A1. Measured, calibrated linear polarization angle for eight features on Venus, compared to the value of the polarization angle expected from subsurface scattering. These measurements are from Venus observations in 2004. The error bars represent the standard deviation of individual χ measurements that went into the average value plotted. If the data fit the subsurface scattering model perfectly, they would lie along the dotted line. The eight features used, from left to right on the graph, are Shukmite Corona, Maxwell Montes, Anya crater, wind streaks near West crater, Stuart crater, Beta Regio, Weil crater, and Xantippe crater. The measured polarization angle for Xantippe (the data point farthest to the right) was wrapped from −1.5 to 1.6 in order to facilitate comparison with the other data points.

[44] **Acknowledgments.** We very much appreciate observing assistance from A. Hine, M. Nolan, P. Perrilat, and the Arecibo Observatory staff. K. Kratter assisted with observations and processing of the 2004 data.

K. Williams and R. Ghent supplied photos of the Sunset Crater Volcano area and provided helpful discussion of the region. E. Stofan and D. Senske gave helpful reviews, which improved the manuscript. Arecibo Observatory is part of the National Astronomy and Ionosphere Center, which is operated by Cornell University under cooperative agreement with the NSF and with support from NASA.

References

Addington, E. A. (2001), A stratigraphic study of small volcano clusters on Venus, *Icarus*, *149*, 16–36.

Arvidson, R. E., R. A. Brackett, M. K. Shepard, N. R. Izenberg, and B. Fegley Jr. (1994), Microwave signatures and surface properties of Ovda Regio and surrounding, Venus, *Icarus*, *112*, 171–186.

Barrick, D. E., and W. H. Peake (1967), Scattering from surfaces with different roughness scales: Analysis and interpretation, *Electrosci. Lab. Rep. 1388–26*, Ohio State Univ., Columbus.

Campbell, B. A. (1994), Merging Magellan emissivity and SAR data for analysis of Venus surface dielectric properties, *Icarus*, *112*, 187–203.

Campbell, B. A., and D. B. Campbell (1992), Analysis of volcanic surface morphology on Venus from comparison of Arecibo, Magellan, and terrestrial airborne radar data, *J. Geophys. Res.*, *97*, 16,293–16,314.

Campbell, B. A., and D. A. Clark (2005), Geologic map of the Mead Quadrangle (V-21) Venus, in *U.S. Geological Survey Atlas of Venus*, in press, U. S. Geol. Surv., Washington, D. C.

Campbell, B. A., and P. G. Rogers (1994), Bell Regio, Venus: Integration of remote sensing data and terrestrial analogs for geologic analysis, *J. Geophys. Res.*, *99*, 21,153–21,171.

Campbell, B. A., and M. K. Shepard (1996), Lava flow roughness and depolarized radar scattering, *J. Geophys. Res.*, *101*, 18,941–19,851.

Campbell, B. A., J. F. Bell III, S. H. Zisk, B. R. Hawke, and K. A. Horton (1992), A high-resolution radar and CCD imaging study of crater rays in Mare Serenitatis and Mare Nectaris, *Proc. Lunar Planet. Sci. Conf.*, *22nd*, 259–274.

Campbell, B. A., T. A. Maxwell, and A. Freeman (2004), Mars orbital synthetic aperture radar: Obtaining geologic information from radar polarimetry, *J. Geophys. Res.*, *109*, E07008, doi:10.1029/2004JE002264.

Campbell, M. J., and J. Ulrichs (1969), Electrical properties of rocks and their significance for lunar radar observations, *J. Geophys. Res.*, *74*, 5867–5881.

Carter, L. M. (2005), Investigating mantling deposits on Venus and regoliths on asteroids using radar polarimetry, Ph.D. thesis, Cornell Univ., Ithaca, New York.

Carter, L. M., D. B. Campbell, and B. A. Campbell (2004), Impact crater related surficial deposits on Venus: Multipolarization radar observations with Arecibo, *J. Geophys. Res.*, *109*, E06009, doi:10.1029/2003JE002227.

Crumpler, L. S., J. C. Aubele, D. A. Senske, S. T. Keddie, K. P. Magee, and J. W. Head (1997), Volcanoes and centers of volcanism on Venus, in *Venus II*, edited by S. W. Bougher, D. M. Hunten, and R. J. Phillips, pp. 697–756, Univ. of Ariz. Press, Tucson.

Fagents, S. A., and L. Wilson (1995), Explosive volcanism on Venus: Transient volcanic explosions as a mechanism for localized pyroclast dispersal, *J. Geophys. Res.*, *100*, 26,327–26,338.

Guest, J. E., M. H. Bulmer, J. Aubele, K. Beratan, R. Greeley, J. W. Head, G. Michaels, C. Weitz, and C. Wiles (1992), Small volcanic edifices and volcanism in the plains of Venus, *J. Geophys. Res.*, *97*, 15,949–15,966.

Hagfors, T., and J. V. Evans (1968), Radar studies of the Moon, in *Radar Astronomy*, edited by J. V. Evans and T. Hagfors, chap. 5, pp. 219–273, McGraw-Hill, New York.

Head, J. W., and L. Wilson (1986), Volcanic processes and landforms on Venus: Theory, predictions, and observations, *J. Geophys. Res.*, *91*, 9407–9446.

Head, J. W., D. B. Campbell, C. Elachi, J. E. Guest, D. P. McKenzie, R. S. Saunders, G. G. Schaber, and G. Schubert (1991), Venus volcanism: Initial analysis from Magellan data, *Science*, *252*, 276–281.

Jackson, J. D. (1999), *Classical Electrodynamics*, 3rd ed., John Wiley, Hoboken, N. J.

Pettengill, G. H., P. G. Ford, and R. J. Wilt (1992), Venus surface radiothermal emission as observed by Magellan, *J. Geophys. Res.*, *97*, 13,091–13,102.

Pettengill, G. H., P. G. Ford, and R. A. Simpson (1996), Electrical properties of the Venus surface from bistatic radar observations, *Science*, *272*, 1628–1631.

Plaut, J. J. (1993), Magellan vertical polarization radar observations (abstract), *Lunar Planet. Sci.*, *XXIV*, 1151–1152.

Rankin, J. M., D. B. Campbell, and S. R. Spangler (1972), 430-Mhz radio astronomical polarimetry at Arecibo Observatory, report, Natl. Astron. and Ionosphere Cent., Cornell Univ., Arecibo, Puerto Rico.

Schaefer, L., and B. Fegley (2004), Heavy metal frost on Venus, *Icarus*, *168*, 215–219.

Shepard, M. K., B. A. Campbell, M. Bulmer, T. Farr, L. R. Gaddis, and J. Plaut (2001), The roughness of natural terrain: A planetary and remote sensing perspective, *J. Geophys. Res.*, *106*, 32,777–32,795.

Stacy, N. J. S. (1993), High-resolution synthetic aperture radar observations of the Moon, Ph.D. thesis, Cornell Univ., Ithaca, New York.

Tryka, K. A., and D. O. Muhleman (1992), Reflection and emission properties on Venus: Alpha Regio, *J. Geophys. Res.*, *97*, 13,379–13,394.

B. A. Campbell and L. M. Carter, Center for Earth and Planetary Studies, Smithsonian Institution, PO Box 37012, Washington, DC 20013, USA. (carterl@si.edu)

D. B. Campbell, Department of Astronomy, Space Sciences Building, Cornell University, Ithaca, NY 14853, USA.